RSC Advances




ROYAL SOCIETY OF CHEMISTRY

www.rsc.org/advances

# Photoluminescence and cathodoluminescence properties of green phosphor $Na_2MgGeO_4:Mn^{2+}$

**Lingzhi Hu, Qian Wang, Xicheng Wang, Yang Li, Yuhua Wang*, Xingping Peng***

*Key Laboratory for Special Function Materials and Structure Design of the Ministry of the Education, School of Physical Science and Technology, Lanzhou University, Lanzhou, 730000, P.R. China.*

*Corresponding authors: Fax:+86 9318913554. Tel: +86 9318912772.

*Corresponding authors E-mail: wyh@lzu.edu.cn, pengxp@lzu.edu.cn.

**Abstract:**

$Mn^{2+}$-doped $Na_2MgGeO_4$ green phosphors were prepared by the solid-state reaction method. X-ray diffraction, scanning electron microscope, photoluminescence (PL) and cathodoluminescence (CL) were utilized to characterize the prepared phosphor. Under UV radiation (297nm), the $Mn^{2+}$-doped phosphor shows a strong green emission corresponding to the $^4T_1(^4G)$– $^6A_1(^6S)$ transition of $Mn^{2+}$ ions. The possible interaction mechanism was investigated. The CL spectra as a function of accelerating voltage and probe current were also measured. Under continuous low-voltage electron-beam excitation, the phosphor exhibits excellent degradation property and good color stability. The results indicate that the phosphor $Na_2MgGeO_4:0.03Mn^{2+}$ can be a suitable green phosphor candidate for FEDs.

**Key Words: FED, phosphor , $Na_2MgGeO_4$**

## 1. Introduction

As ken Shoulder proposed the idea of an electron beam micro-device based on Field Emissive Arrays in the 1960s, a rapid development on flat panel displays(FPDs) have been happened.[1, 2] As one of the most promising candidates for next generation of FPDs, Field emission displays(FEDs) have attracted much attention due to their potential performances such as distortion-free image, wide viewing angle, thin panel thickness, self-emission, low power consumption, and quick response.[3, 4] By employing the similar operation principles of conventional cathode ray tubes, FEDs utilize cathode rays to excite phosphors on anode. But FEDs have no deflection coils, so they can be very thin and should work with low-voltage electrons (<5kV). [3, 5, 6] As we all known, the low-voltage will decrease the CL intensity of phosphors, in order to solve the problem high current density (10-100μA$cm^{2-}$) should be adopted.[7-9] Thus it is important to develop FED phosphors with highly luminescent efficiency and excellent conductivity under low-voltage electrons and high current density. The traditional sulfide-based phosphors such as $Y_2O_2S$: Eu, $SrGa_2S_4$: Eu, Zn(Cd)S: Cu, Al, ZnS: Ag, Cl, have been developed as possible FED phosphors for highly luminescence efficiency and considerable conductivity. [10] However, sulfide phosphors degrade significantly and release harmful gases under high-energy electron bombardment. This will poison the cathodes and shorten the device lifetime subsequently.[11, 12] In order to improve device performance and lifetime of the FEDs, it is necessary to find novel phosphors with highly luminescence efficiency, excellent color rendering properties and superior stability under electron bombardment. Oxide-based phosphors have attracted great

interest due to their good chemical and thermal stability, which is more environmental friendly in comparison with sulfides. Moreover, they show highly efficiency, color rendering and good stability under low-voltage electron beam excitation[13]. Germanates have all the advantages of oxide-based hosts, and they also have potential applications on electronic, photodetectors, electroluminescence and so on.[14-16] Especially in recent years, the cathodoluminescence properties of germanates attract many attentions. Lin et al. investigated red phosphor $Ca_2GeO_4:Eu^{3+}$, green phosphors $Li_2ZnGeO_4:Mn^{2+}$ [17] and $Zn_2GeO_4:Mn^{2+}$ [18-20] for FEDs, thus the germinates exist possibility to apply for FEDs, however they still cannot satisfy the application until now, thus more investigation should be done. Moreover, morphology and size can influence the cathodoluminescence properties of phosphors.[21] The regular morphologies, such as spherical morphology, are beneficial to give higher packing densities. Furthermore, small particle size is advantageous to achieve higher resolution.[22, 23] For phosphors, a befitting host should have a befitting luminescence center, thus a suitable doping-ion is important. $Mn^{2+}$ ion is a significant activator often used in FED phosphors. $Mn^{2+}$ usually shows a broad band emission due to the $^4T_1(^4G)$-$^6A_1(^6S)$ transition. With the d electrons within the 3d shell, $Mn^{2+}$ emission can be affected by the crystal field strongly with the emission shifting from green to red.[24, 25] Such as green phosphors $Li_2ZnGeO_4:Mn^{2+}$ [17], $(Zn, Mg)_2GeO_4:Mn^{2+}$ [18] , $Mg_2SnO_4:Ti^{4+},Mn^{2+}$ [26] , yellow phosphor $NaCaPO_4:Mn^{2+}$ [27] , $Ca_2Gd_8(SiO_4)_6:Mn^{2+}$ [28] and red phosphor $AlN:Mn^{2+}$ [29], $Sr_3In(PO_4)_3:Mn^{2+}$ [30], $Mg_2Y_8(SiO_4)_6O_2:Mn^{2+}$ [31], $Ca_4Y_6(SiO_4)_6O:Mn^{2+}$ [32].

As a Germanate, $Na_2MgGeO_4$ is isostructural to $Na_2ZnGeO_4$, which has a monoclinic space group P1n1. The $Mn^{2+}$-doped $Na_2MgGeO_4$ phosphor has been reported by Asish Kumar Sharma[33], which concentrates on the application in cold cathode fluorescent lamp and no available information on the application in the FEDs can be found. Moreover, as the author paid more attention on the multi-objective genetic algorithm-assisted combinatorial method, there was little information about luminescence except its photoluminescence emission spectra. Therefore, in this work, we employed solid-state reaction to prepare $Na_2MgGeO4:Mn^{2+}$ phosphor, and then investigated its PL properties and CL properties in detail for fundamental research and the potential application in FED devices.

## 2.Experimental section

### 2.1Preparation.

$Na_2Mg_{1-x}GeO_4:xMn^{2+}$ ($0.005 \leqslant x \leqslant 0.06$) powders were synthesized by solid-state reaction method. The starting materials $Na_2CO_3$(A.R.), $4MgCO_3 \cdot Mg(OH)_2 \cdot 5H_2O$ (A.R.), $GeO_2$ (A.R.), and $MnCO_3$(A.R.) were weighed stoichiometrically and grounded thoroughly in an agate mortar, and then sintered in aluminium oxide($Al_2O_3$) crucibles at 950℃ for 6h under a reductive atmosphere ($N_2/H_2$=40:5) in a tube furnace:

$$5Na_2CO_3 + (1-x)4MgCO_3 \cdot Mg(OH)_2 \cdot 5H_2O + 5xMnCO_3 + 5GeO_2 \rightarrow 5Na_2Mg(1-x)GeO_4:xMn + (9+x)CO_2 + 6(1-x)H_2O$$

Finally the as-synthesized samples were cooled down to room temperature and grounded again for future measurement.

### 2.2Characterization

The crystal structure was identified by using a Bruker X-ray diffractometer (XRD) (D2 PHASER X-ray Diffractometer, Germany) with Ni-filtered Cu Kα radiation (λ=1.54056Å, scan rate=15° /min, range from 10° to 80° ). The morphologies were observed by field emission scanning electron microscopy (FESEM, Hitachi, S-4800). The photoluminescence (PL) and PL excitation (PLE) spectra of the samples were measured by using an FLS-920T fluorescence spectrophotometer equipped with a 450 W xenon light source. The cathodoluminescence properties of the samples were obtained using a modified Mp-Micro-S instrument. All of the measurements were performed at room temperature.

## 3.Results and discussion

### 3.1 phase identification and morphology

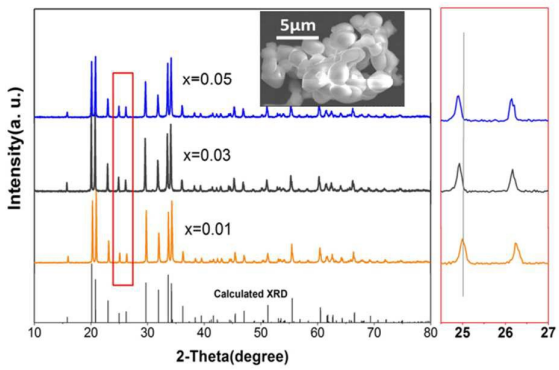


**Fig. 1** XRD patterns of $Na_2MgGeO_4$:0.01$Mn^{2+}$, $Na_2MgGeO_4$:0.03$Mn^{2+}$,and $Na_2MgGeO_4$:0.05$Mn^{2+}$ (the Calculated XRD data of $Na_2MgGeO_4$ is shown as reference).The right part is the magnified area of the red box and the inset is the SEM image of the $Na_2MgGeO_4$:0.03$Mn^{2+}$.

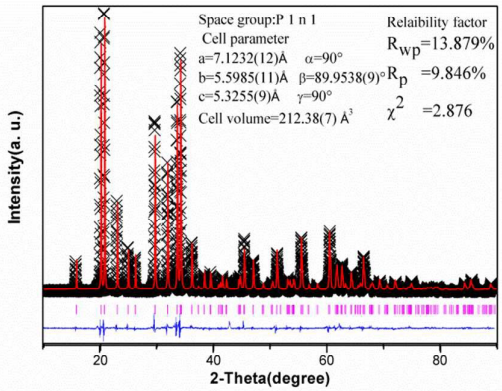


**Fig. 2** Observed (crossed), calculated (red line) XRD pattern and the difference profile (bule line) of the Rietveld refinement of $Na_2MgGeO_4$:0.03$Mn^{2+}$. Bragg reflection is shown as vertical bars. Inset shows the fit parameters.

Fig. 1 shows a series of XRD patterns for $Na_2MgGeO4$ :$Mn^{2+}$ ($0 \le x \le 0.06$) phosphors with different doping concentration(the XRD patterns of other samples are similar) as well as the calculated XRD patterns according to the crystal structure parameters of $Na_2MgGeO_4$:$Mn^{2+}$.[33] No detectable impurity phase can be observed in the obtained samples. The XRD profiles are well fitted with the calculated XRD patterns, indicating that all of the samples are single phase and the $Mn^{2+}$ ions have been successfully incorporated in the $Na_2MgGeO_4$ host lattice without changing the crystal structure obviously. Moreover, it is found that the XRD diffraction angle of the studied $Na_2MgGeO_4$:$Mn^{2+}$ samples gradually decrease with the increase of $Mn^{2+}$ ions doping content due to the larger ionic radius of $Mn^{2+}$ with respect to $Mg^{2+}$. This can indicates that the $Mn^{2+}$ ions have replaced the $Mg^{2+}$ lattice sites in the $Na_2MgGeO_4$ host.

Similarly, the morphology of the $Na_2MgGeO_4$:0.03$Mn^{2+}$ sample prepared by solid-state reaction is presented in the inset of Fig. 1(as a representative sample). The $Na_2MgGeO_4$:0.03$Mn^{2+}$ sample consists of spherical-like particles with sizes ranging from 1 to5μm, the surface of the particles is smooth, but agglomerating with each other. The spherical-like particles gained at relatively low temperature 950°C can be attributed to the starting materials $4MgCO_3 \cdot Mg(OH)_2 \cdot 5H_2O$ and $NaCO_3$, of which fusion point is 350°C and 851°C respectively. They can play the role of flux, then melted and covered other components to form this spherical-like particles, and also result in the serious agglomeration.[34] The obtained spherical-like

morphology and size of this sample are beneficial for producing a compact phosphor screen and also improving its CL property. [35, 36]

Fig. 2 shows Rietveld structural refinements of the powder diffraction patterns of $Na_2MgGeO_4$:0.03$Mn^{3+}$. The structural parameter reported in reference 26 was used as initial parameter in the Rietveld analysis. Structural refinement of $Na_2MgGeO_4$:0.03$Mn^{2+}$ indicated that it crystallizes in a monoclinic crystal system with the space group P1n1 with the following unit cell parameters: $a$ = 7.123(12) Å, $b$ = 5.5985(11) Å, $c$ = 5.325(9) Å, $\beta$ = 89.954(9)° ,$V$ (cell volume) = 212.98(7) Å$^3$ . The reliability parameters of refinements are $R_p$ = 13.879%, $R_{wp}$ = 9.846%, and $\chi^2$ = 2.88. Fig.3 shows the crystal structure of $Na_2MgGeO_4$.It can be seen that the structure framework of $Na_2MgGeO_4$:0.03$Mn^{3+}$ lattice is built up by $GeO_4$ tetrahedra and $MgO_4$ tetrahedra which connecting with each other through sharing corner. $Na^+$ ions in this schematic occupy two positions: one is forming an almost regular tetrahedron with four oxygen ions, and another is surrounded by six oxygen ions.[37]

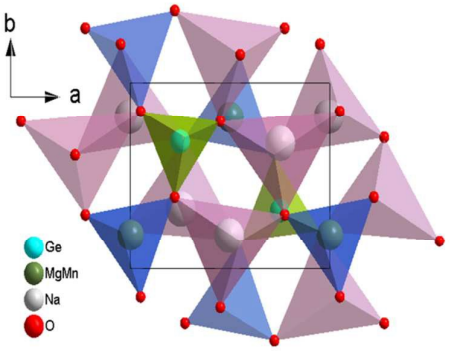


**Fig. 3** Crystal structure of $Na_2MgGeO_4$

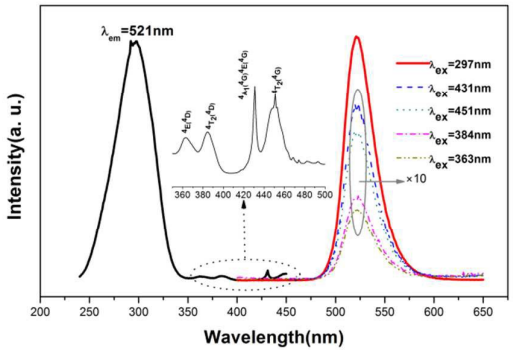


**Fig. 4** The PLE and PL spectra of $Na_2MgGeO_4$:0.03$Mn^{2+}$.The magnified part reveals the excitation spectrum in the range of 350-500nm.

### 3.2 Photoluminescence properties

Fig. 4 shows the PLE and PL spectra of the $Na_2MgGeO_4$:0.03$Mn^{2+}$ phosphor. Under 297 nm excitation, the as-prepared $Na_2MgGeO_4$:0.03$Mn^{2+}$ phosphor shows a strong green emission band ranging from 475nm to 550nm centering at 521nm, which can be ascribed to the $^4T_1(^4G)$– $^6A_1(^6S)$ transition of the $Mn^{2+}$ ions.[38] When monitoring emission at 521nm, there are a broad strong excitation band ranging from 240nm to 350nm with the maximum at 297 nm and several weak sharp peaks at 363nm, 384nm, 431nm, and 451nm, which are attributed to the transitions from $^6A_1(^6S)$ to $^4E(^4D)$, $^4T_2(^4D)$, [$^4A_1(^4G)$, $^4E(^4G)$] and $^4T_2(^4G)$ respectively. Due to the d–d transitions are spin and parity forbidden, the excitation bands in the wavelength range of 350–500 nm are very weak, which agrees well with emission spectra(10 × magnified emission spectra). Meanwhile, the emission spectra do not change under different wavelengths excitation, thus indicate that there is only one luminescence center in this host, which agrees well with $Mn^{2+}$ occupies $Mg^{2+}$ position.

The dependence of PL intensity on the $Mn^{2+}$ concentration was also investigated, shown in Fig. 5. It can be seen that the PL intensity rapidly increases with the $Mn^{2+}$ content increasing from 0.005 to 0.03, and reaches a maximum at about 0.03. Above this content, concentration quenching occurs.

The concentration quenching is associated with the critical energy transfer distance between $Mn^{2+}$ ions. The critical distance(Rc) of $Mn^{2+}$ ions is determined by the following formula given by Blasse[39]

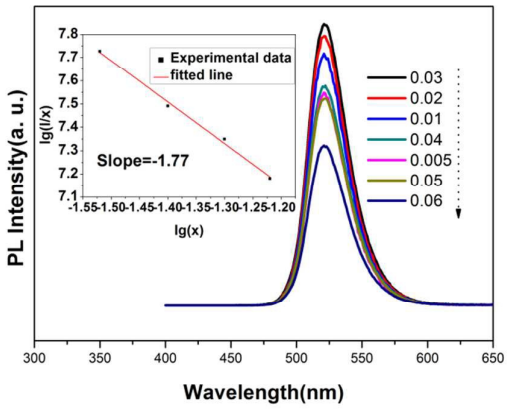


**Fig. 5** PL spectrum of samples $Na_2MgGeO_4$:x$Mn^{2+}$($0 \le x \le 0.06$).Inset: The dependence of lg(I/$x$) on lg($x$).

$$Rc \approx 2[\frac{3V}{4\chi_c \pi N}]^{\frac{1}{3}}$$

Where $V$ is the volume of the unit cell, $\chi_c$ is the critical concentration of $Mn^{2+}$ ions and $N$ is the number of cations substituted by $Mn^{2+}$ ions in the unit cell. The values of $N$, $\chi_c$ and $V$ for the $Na_2MgGeO_4$ host are 2, 0.03, and 212.38 $Å^3$, respectively. So the Rc value is approximately 21.70 Å. Moreover, the possible interaction mechanism was investigated, for the critical distance is longer than 5Å, which indicates that interaction mechanism couldn't result from exchange interaction[40]. According to Dexter's theory[41], it can be confirmed that the concentration quenching is caused by the multipolar–multipolar interactions. The interaction type can be determined by the following Eq

$$\frac{I}{x} = K[1 + \beta(x)^{\theta/3}]^{-1}$$

where $I$ means the emission intensity, $x$ is the concentration of activator, $K$ and $\beta$ are constants under the same excitation for a given matrix. The value of $\theta$ equals to 6, 8, or 10 and represents the dipole–dipole, dipole–quadrupole, or quadrupole–quadrupole interaction mechanism, respectively. As x exceeds the critical concentration, a simple equation can be used:

$$\frac{I}{x} = K'[\beta(x)^{\theta/3}]^{-1}$$

For this part, the ratio of lg(I/x ) and lg(x) equals to the value of ($-\theta/3$). According to the inset of Fig.5, the ratio is -1.77, which means the value of $\theta$ is close to 6. So the concentration quenching of $Mn^{2+}$ ions in $Na_2MgGeO_4$ host should originate from dipole-dipole interacting.

### 3.3 CL properties of $Na_2MgGeO_4$: $Mn^{2+}$.

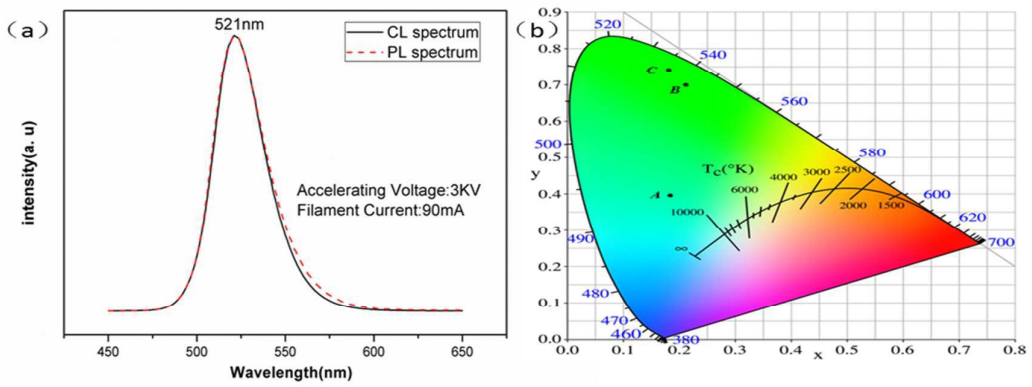


**Fig.6** (a)The CL spectrum and PL spectrum of the $Na_2MgGeO_4$:0.03$Mn^{2+}$ sample (b)The CIE chromaticity diagram for ZnO:$Zn^{2+}$(A),$Zn_2SiO_4$:$Mn^{2+}$(B) and $Na_2MgGeO_4$:0.03$Mn^{2+}$(C)

To explore its potential use as FED materials, the Cl properties have been investigated in detail. Fig.6 (a) shows the CL spectrum and PL spectrum of $Na_2MgGeO_4$:$Mn^{2+}$ sample. Under low-voltage electron-beam excitation (90mA , 3kV), the $Na_2MgGeO_4$:$Mn^{2+}$ shows broad emission ranging from 475nm to 600nm with a maximum at 521nm, which is similar to its PL spectrum. The broad emission is also ascribed to the $^4T_1(^4G)$– $^6A_1(^6S)$ transition of the $Mn^{2+}$ions. For FEDs, the color purity of phosphor is an important index for the practical application. The full width at half maximum(FWHM) of the CL spectrum is about 35nm， which reveals high color purity and excellent chromaticity coordinate characteristics. In order to evaluate the color purity of the prepared phosphor, we compared the CIE chromaticity coordinates with those of ZnO: $Zn^{2+}$ and $Zn_2SiO_4$:$Mn^{2+}$. It can be seen in Fig.6(b), A, B and C refers to ZnO:$Zn^{2+}$， $Zn_2SiO_4$:$Mn^{2+}$ and $Na_2MgGeO_4$:$Mn^{2+}$ respectively. ZnO: $Zn^{2+}$ shows a whitish-green emission and $Zn_2SiO_4$:$Mn^{2+}$ shows a highly pure green emission while $Na_2MgGeO_4$:$Mn^{2+}$ even has a better green emission than them. The CIE color coordinates of $Na_2MgGeO_4$:$Mn^{2+}$ are x = 0.172 and y = 0.745.

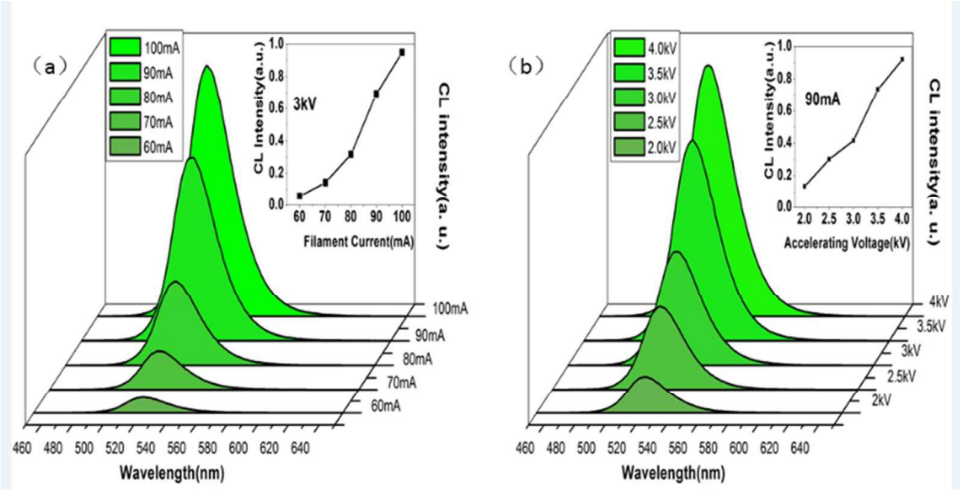


**Fig.7** CL intensity of the $Na_2MgGeO_4$:0.03$Mn^{2+}$ samples as a function of accelerating voltage(a) and filament current(b) . The insets clearly show their relationship, all of them are taken at 521nm.

The CL emission spectra has been investigated as a function of the accelerating voltage and the filament current, as shown in Fig.7. When the accelerating voltage fixed at 3kV, the CL

intensity increases with raising the filament current from 60mA to 100mA, no saturation effect can be observed. As mentioned above, FEDs utilize low-voltage electrons (<5kV) to suits for the thinner panel, which will also reduce the CL intensity of phosphors. Thus in order to enhance the CL intensity of the FEDs, high current should be adopted. The CL intensity will increase along with the increasing of filament current. However as the filament current exceeds the threshold, the CL intensity will increase no longer or even decline, which is called saturation effects.[7] Wagner and co-works have discussed the factors affecting the performance of low voltage CL phosphors. They found there is a lot factors influence it such as electron penetration, diffusion length, surface recombination, and activator decay rates and so on. [42]Saturation effect is also an important factor which hinders phosphors applying on FEDs, thus the FED phosphors should have a high saturation current. As shown in Fig.7, the CL intensity continuously increases with increasing beam current, indicating that the phosphor is resistant to the current saturation, which is of benefit to FEDs.

Similarly, under a 90mA filament current excitation, the CL intensity also increases with increasing the accelerating voltage from 2 to 4kV (Fig. 7b). Incident electrons hitting on the surface of the phosphors will produce kinds of secondary electrons. As most of the secondary electrons lack of energy, they will be scattered. Thus the penetration of the secondary electrons is superficial and the CL intensity is reduced for the surface defects. With increasing the accelerating voltage, the incident electrons have higher energy, thus the increase in CL brightness is attributed to the deeper penetration of the electrons into the phosphor body. The deeper the electron penetration depth, the more plasma will be produced, which results in more doped-ions being excited and thus, the CL intensity increases.[12] The electron penetration depth can be estimated using the empirical formula:[43]

$$\mathrm{L}(\text{Å}) = 250(A/\rho)(E/Z^{1/2})^{n}$$

$$n = 1.2/(1-0.29\lg Z)$$

According to the equation, $A$ is the atomic or molecular weight of the material, $Z$ is the atomic number or the number of electrons per molecule in the compounds,$\rho$ is the bulk density, and $E$ is the accelerating voltage (kV). For $Na_2MgGeO_4$, $Z$=98, $A$=206.5, $\rho$ =3.23g/cm$^{-3}$, the estimated electron penetration depth at 2, 3 and 4kV are 17.02nm, 53.84nm, 121.90nm, respectively. Furthermore, the CL spectrum maxima keep almost the same with the peak location at 521 nm when changing the accelerating voltage and the filament current.

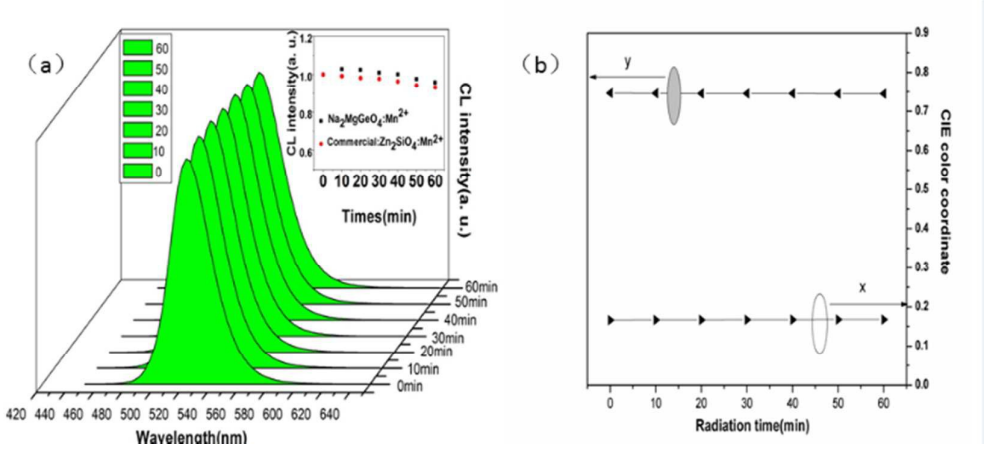


**Fig.8** (a)CL intensity of the Na2MgGeO$_4$:0.03Mn$^{2+}$ on the radiation time（accelerating voltage=3.0kV,filament current=90mA）.The inset show their relationships.(b)The CIE color coordinates of Na2MgGeO$_4$:0.03Mn$^{2+}$.

The degradation property of phosphor is very important for FED application. The electron-beam radiation will reduce the CL intensity after radiating some time, for it makes the permanent damage on the surface of phosphors. Moreover, the color stability is also facing a challenge.[22] Thus we also investigated the degradation behavior of $Na_2MgGeO_4$:0.03$Mn^{2+}$ sample under continuous low-voltage electron-beam excitation and this is illustrated in Fig. 8(a). The accelerating voltage was kept at 3.0kV and the filament current was 90mA. For comparison, the degradation property of the commercial $Zn_2SiO_4$:$Mn^{2+}$ was also measured. After continuous electron radiation for 1h,the CL intensity of the $Na_2MgGeO_4$:0.03$Mn^{2+}$ remains 95.2% and the CL intensity of $Zn_2SiO_4$:$Mn^{2+}$ falls to 93.1% of their initial values. For most phosphors used in FEDs, the CL intensity decreased consecutively with the increase of the bombing times. This is due to the accumulation of carbon at the surface during electron bombardment. During continuous electron bombardment, graphitic carbon will accumulate on the surface of phosphors and cause the well-known effect of carbon contamination, which will exacerbate surface charging, and thus lower the CL intensity.[44] In this test, after continuous electron radiation for 1h $Na_2MgGeO_4$:0.03$Mn^{2+}$ shows better degradation resistance properties than the commercial phosphor. Moreover, in this case, an interesting phenomenon is worth noticing. The degradation curve of $Na_2MgGeO_4$:0.03$Mn^{2+}$ phosphor was not falls consecutively but a slight increase after 10min bombing. According to Wu and co-worker investigation, this abnormal degradation behavior could be caused by the increase of the specific surface area.[45] It is well known that the CL intensity will increase as the bombarding surface area increased, also the degradation behavior will appear after continuous electron radiation .When the effect of specific surface area increasing overcomes degradation behavior, an increasing curve appears, and vice versa.

Similarly，the CIE color coordinates of the $Na_2MgGeO_4$:0.03$Mn^{2+}$ phosphor under a continuous electron-beam radiation with different radiation time (min) were also measured to investigate the color stability, as presented in Fig. 8(b). The CIE values were nearly invariable under a continuous electron radiation for 1h. X and y remained at about 0.17 and 0.74, respectively. In summary, the short time experiment indicated that the stability of the CL intensity and CIE color coordinate of the $Na_2MgGeO_4$:0.03$Mn^{2+}$ samples are good, which shows potential advantages applied in the FED.

## 4. Conclusion

In summary, $Mn^{2+}$ doped $Na_2MgGeO_4$ phosphors with spherical-like morphology were prepared by solid-state reaction. The PL and CL properties were investigated in detail. Under UV or electron beam, the samples showed highly bright green emission, which is ascribed to $^4T_1(^4G)$–$^6A_1(^6S)$ transition of the $Mn^{2+}$ ions. The concentration quenching was investigated and the possible interaction mechanism between $Mn^{2+}$ ions in $Na_2MgGeO_4$ host is dipole–dipole interaction under UV radiation. The CL intensity increased with the increase of acceleration voltage from 2 to 4kV for the deeper electron penetration depth. And with the increase of filament current from 60mA to 100mA, no saturation trend can be observed. Moreover, the $Na_2MgGeO_4$:0.03$Mn^{2+}$ exhibits a higher color purity and better degradation behavior than $Zn_2SiO_4$:$Mn^{2+}$ phosphor. After a continuous electron radiation for 1h,the CL intensity remains 95.2% and the CIE coordinates are nearly invariable. These excellent CL properties indicate that $Na_2MgGeO_4$:0.03$Mn^{2+}$ has great

potential as a green phosphor for full color FEDs.

**Acknowledgements**

This work was supported by the National Natural Science Funds of China (Grant No. 51372105) and Gansu Province Development and Reform Commission.

**Notes and references**

1 K. R. Shoulders, *Adv. Computers*, 1961, ***2***, 135.

2 C. Liu, S. Zhang, Z. Liu, H. Liang, S. Sun and Y. Tao, *J. Mater. Chem. C*, 2013, ***1***, 1305.

3 S. Itoh, M. Tanaka and T. Tonegawa, *J. Vac. Sci. Technol. B* ,2004, ***22***, 1362-1366.

4 A. Mao, Z. Zhao, Y. Wang, Q. Wu, X. Wang, C. Wang and Y. Li, *ECS Solid State Lett.,* 2015, ***4***, R17-R21.

5 S. Zhang, H. Liang, Y. Liu, Y. Liu, D. Hou, G. Zhang and J. Shi, *Opt. Lett.,* 2012, ***37***, 2511-2513.

6 L. E. Shea, *ECS inter.,* 1998, ***7***, 24-27.

7 P. H. Holloway, T. A. Trottier, B. Abrams, C. Kondoleon, S. L. Jones, J. S. Sebastian, W. J. Thomes and H. Swart, *J. Vac. Sci. Technol., B* ,1999, ***17***, 758.

8 S. H. Cho, S. H. Kwon, J. S. Yoo, C. W. Oh, J. D. Lee, K. J. Hong and S. J. Kwon, *J. Electrochem. Soc.,* 2000, ***147***, 3143-3147.

9 M. H. Lee, S. G. Oh, S. C. Yi, D. S. Seo, J. P. Hong, C. O. Kim, Y. K. Yoo and J. S. Yoo, *J. Electrochem. Soc.,* 2000, ***147***, 3139-3142.

10 S. Itoh, T. Kimizuka and T. Tonegawa, *J. Electrochem. Soc.,* 1989, ***136***, 1819-1823.

11 H. Swart, J. Sebastian, T. Trottier, S. Jones and P. Holloway, *J. Vac. Sci. Technol., A* ,1996, ***14***, 1697-1703.

12 G. Li, C. Li, C. Zhang, Z. Cheng, Z. Quan, C. Peng and J. Lin, *J. Mater. Chem.,* 2009, ***19***, 8936-8943.

13 G. Zhu, Z. Ci, Q. Wang, Y. Wen, S. Han, Y. Shi, S. Xin and Y. Wang, *J. Mater. Chem. C*, 2013, ***1***, 4490.

14 J. Bender, J. Wager, J. Kissick, B. Clark and D. Keszler, *J. Lumin.,*2002, ***99***, 311-324.

15 M. Yu, J. Lin, Y. Zhou and S. Wang, *Mater. Lett.,*2002, ***56***, 1007-1013.

16 L. Li, P. S. Lee, C. Yan, T. Zhai, X. Fang, M. Liao, Y. Koide, Y. Bando and D. Golberg, *Adv. Mater.,* 2010, ***22***, 5145-9.

17 M. Shang, G. Li, D. Yang, X. Kang, C. Peng and J. Lin, *Dalton Trans.,* 2012, ***41***, 8861.

18 Q. Zhang and J. Wang, *Appl. Phys. A,* 2012, ***108,*** 943-948.

19 M. Shang, G. Li, D. Yang, X. Kang, C. Peng, Z. Cheng and J. Lin, *Dalton Trans.,* 2011, ***40***, 9379-87.

20 L. C. Williams, D. Norton, J. Budai and P. H. Holloway, *J. Electrochem. Soc.,* 2004, ***151***, H188.

21 G. Li and J. Lin, *Chem. soc. Rev.,* **2014**, *43*, 7099-7131.

22 D. Geng, G. Li, M. Shang, C. Peng, Y. Zhang, Z. Cheng and J. Lin, *Dalton Trans.,* **2012**, *41*, 3078-3086.

23 G. Li, Z. Hou, C. Peng, W. Wang, Z. Cheng, C. Li, H. Lian and J. Lin, *Advanced Functional Materials* **2010**, *20*, 3446-3456.

24 M. Takesada, M. Osada and T. Isobe, *J. Phys. Chem. Solids,* 2009, ***70***, 281-285.

25 A. K. Sharma, K. H. Son, B. Y. Han and K.-S. Sohn, *Adv. Funct. Mater.,* 2010, ***20***, 1750-1755.

26 G. Li, X. Zhang, C. Peng, M. Shang, D. Geng, Z. Cheng and J. Lin, *J. Mater. Chem.,* 2011, ***21***, 6477.

27 G. Li, X. Xu, C. Peng, M. Shang, D. Geng, Z. Cheng, J. Chen and J. Lin, *Opt. Express,* 2011, ***19***, 16423-16431.

28 G. Li, D. Geng, M. Shang, C. Peng, Z. Cheng and J. Lin, *J. Mater. Chem.,* **2011**, *21*, 13334-13344.

29 X. J. Wang, R. J. Xie, B. Dierre, T. Takeda, T. Suehiro, N. Hirosaki, T. Sekiguchi, H. Li and Z. Sun, *Dalton Trans.,* 2014, ***43***, 6120.

30 D. Geng, G. Li, M. Shang, D. Yang, Y. Zhang, Z. Cheng and J. Lin, *J. Mater. Chem.,* **2012**, *22*, 14262-14271.

31 G. Li, D. Geng, M. Shang, Y. Zhang, C. Peng, Z. Cheng and J. Lin, *J. Phys. Chem. C,* **2011**, *115*, 21882-21892.

32 G. Li, Y. Zhang, D. Geng, M. Shang, C. Peng, Z. Cheng and J. Lin, *ACS Applied Mater & Interfaces,* **2011**, *4*, 296-305.

33 A. K. Sharma, C. Kulshreshtha and K.-S. Sohn, *Adv. Funct. Mater.,* 2009, ***19***, 1705-1712.

34 M. Zribi, M. Kanzari and B. Rezig, *Mater. Lett.,* 2006, ***60***, 98-103.

35 M. Zhang, X. Wang, H. Ding, H. Li, L. Pan and Z. Sun, *Int. J. Appl. Ceram. Tec.,* 2011, ***8***, 752-758..

36 L. Shea, J. McKittrick and M. Phillips, *J. Electrochem Soc.,* 1998, ***145***, 3165-3170.

37 Y. Jin, Y. Hu, Y. Fu, G. Ju, Z. Mu, R. Chen, J. Lin and Z. Wang, *J. Am. Ceram. Soc.*, 2015, ***98***, 1555-1561.

38 K. Uheda, T. Maruyama, H. Takizawa and T. Endo, *J. Alloys Compd.,* 1997, ***262***, 60-64.

39 G. Blasse, *Phys. Lett. A,* 1968, ***28***, 444-445

40 S. Xin, Y. Wang, Z. Wang, F. Zhang, Y. Wen and G. Zhu, *Electrochem. Solid-State Lett.,* 2011, ***14***, H438-H441.

41 D. L. Dexter, *J. Chem. Phys.,* 1967, ***47***, 1379.

42 C. Stoffers, S. Yang, S. M. Jacobsen and C. J. Summers, *J. Soc. Inf. Display,* 1996, ***4***, 337-341.

43 C. Feldman, *Phys. Rev.,* 1960, ***117***, 455.

44 G. Zhu, Z. Ci, Y. Shi, M. Que, Q. Wang and Y. Wang, *J. Mater. Chem. C*, 2013, ***1***, 5960.

45 Q. Wu, X. Wang, Z. Zhao, C. Wang, Y. Li, A. Mao and Y. Wang, *J. Mater. Chem. C*, 2014, **2**, 7731-7738.

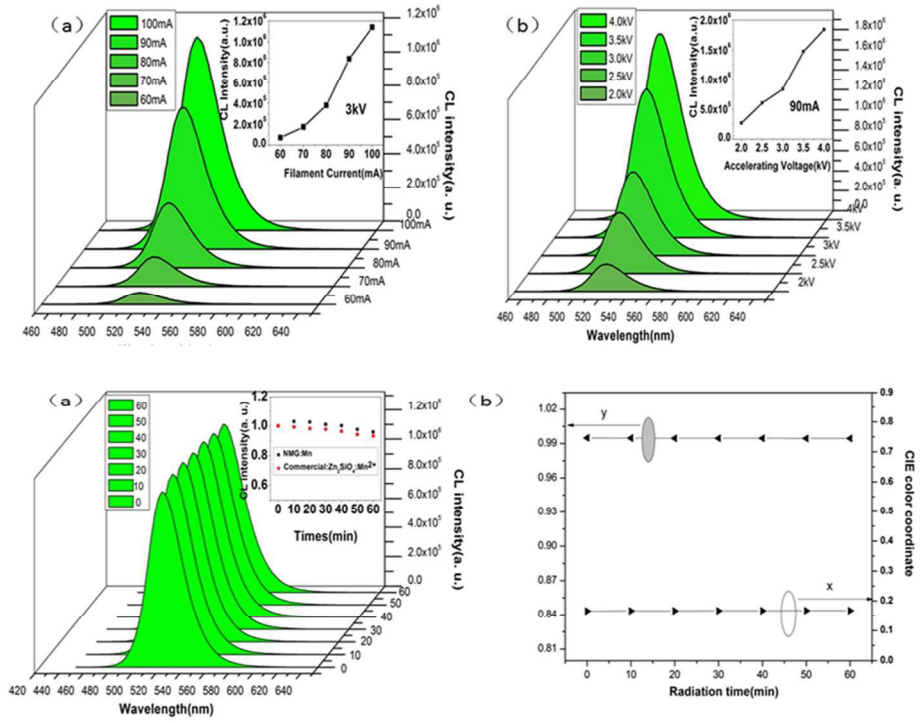


254x190mm (96 x 96 DPI)